Self-Calibration of Large Scale Camera Networks

Patrik Goorts, Steven Maesen, Yunjun Liu, Maarten Dumont, Philippe Bekaert, Gauthier Lafruit
Hasselt University - tUL - iMinds
Expertise Centre for Digital Media
Wetenschapspark 2
3590 Diepenbeek, Belgium
{*patrik.goorts, steven.maesen, yunjun.liu, maarten.dumont, philippe.bekaert, gauthier.lafruit*}*@uhasselt.be*

Keywords: Calibration, Feature Matching, Multicamera Matches, Outlier Filtering

Abstract: In this paper, we present a method to calibrate large scale camera networks for multi-camera computer vision applications in sport scenes. The calibration process determines precise camera parameters, both within each camera (focal length, principal point, etc) and inbetween the cameras (their relative position and orientation). To this end, we first extract candidate image correspondences over adjacent cameras, without using any calibration object, solely relying on existing feature matching computer vision algorithms applied on the input video streams. We then pairwise propagate these camera feature matches over all adjacent cameras using a chained, confident-based voting mechanism and a selection relying on the general displacement across the images. Experiments show that this removes a large amount of outliers before using existing calibration toolboxes dedicated to small scale camera networks, that would otherwise fail to work properly in finding the correct camera parameters over large scale camera networks. We succesfully validate our method on real soccer scenes.

1 INTRODUCTION

In the current multimedia landscape, entertainment delivery in the living room is more important than ever. Users expect more and more impressive content to stay entertained. Therefore, new technologies have been developed, such as 3D television, graphical effects in movies, interactive television, and more.

We will focus on a single use case of novel content creation, i.e. computer vision applications in soccer scenes. In this application, a large number of cameras are placed around the field, creating a large scale camera network. These cameras are then used to generate novel virtual viewpoints (Goorts et al., 2014) or create tracking information of the players on the field.

To make such applications possible, the cameras should be geometrically calibrated, i.e. their intrinsic properties (focal length, principal point, etc) as well as their relative position and orientation (extrinsic parameters) should be estimated (Hartley and Zisserman, 2003, page 178). For small scale camera networks many approaches exist for intrinsic and extrinsic calibration under controlled conditions. Most of them work by moving calibration objects in front of the cameras, such as checker board patterns (Zhang, 2000) and laser lights (Svoboda et al., 2005), providing corresponding feature points in the respective camera views for extracting intrinsics and extrinsics, as explained in section 3.

In this paper, we will present a system to calibrate a large scale camera network placed around the pitch of a sport scene, here demonstrated in a soccer game. We demonstrate our method using eight cameras, but any arbitrary number of cameras can be used. Because access to the pitch is restricted and the scale is very large, we will present a self-calibration system that does not use any calibration objects, such as the methods of Ohta et al. (2007) and Grau et al. (2005).

The main contribution of this paper is the generation of reliable multicamera image correspondences with a minimum of outliers, for efficient self-calibration. This avoids a calibration recording process, reducing cost and effort. These correspondences are used in calibration toolboxes intended for small scale camera networks. We use the toolbox of Svoboda et al. (2005) for estimating the intrinsic and extrinsic parameters.

Correspondence determination and matching is typically used between two images. Features are detected out of each image separately, and their statistical descriptors are pairwise matched between two images. This will, however, not suffice for our applica-

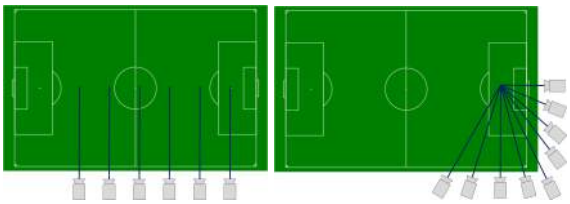

(a) (b)

Figure 1: Two possible camera arrangements for soccer scenes. Both arrangements have different properties. (a) In the linear arrangement, all cameras are placed on a line next to the long side of the pitch and have the same look-at angle. (b) In the curved arrangement, all cameras are placed around a corner of the pitch and point to a spot in the scene.

tion, where feature matches between multiple images are required. Therefore, we present a system to generate multicamera matches by propagating the matches between successive pairs of images.

These multicamera matches might, however, be unreliable. Therefore, we also present a filtering approach that is specifically tailored to cameras placed next to each other, without a relative rotation around their optical axes. Even large scale, curved camera pathways can be properly handled by following a piecewise linear approach over each triple of adjacent camera views. We remove many outliers that would not be removed with existing calibration tools, effectively improving the calibration quality.

There are a number of existing camera calibration methods available for outdoor sport scenes that do not use calibration objects. Most of these methods use the lines of the soccer area to determine camera locations (Farin et al., 2005, 2003; Hayet et al., 2005; Li and Luo, 2004; Thomas, 2007; Yu et al., 2009). They are therefore only applicable if the scene is a soccer pitch, where the lines are planar and visible over all camera views. This is, however, not always the case. The pitch is seldom a plane and cameras with a small field of view do not always have lines in their image stream. We therefore propose a solution without this planar line assumption, which makes our large-scale calibration solution more robust and more widely applicable, with good self-calibration performances (i.e. not requiring any specific calibration object).

The rest of the paper is structured as follows. Section 2 describes the used camera setup, with its geometrical properties recorded into camera matrices, as explained in section 3. Section 4 discusses the generation of the multicamera correspondences and their propagation over adjacent cameras. Finally, section 5 describes our multicamera filtering approach to further dismiss apparant outliers.

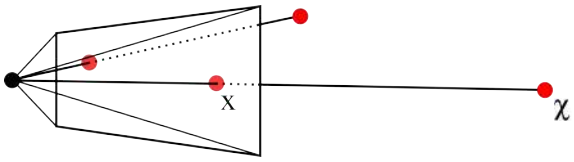

Figure 2: The projective camera model. A camera center and an image plane is defined. The image is formed by connecting a line between the camera center and the 3D point. The intersection between this line and the image plane defines the position of the projection for that 3D point.

2 CAMERA SETUP

We do not present a camera calibration method for all possible camera setups. Instead, we will present a camera method for a large scale camera network, with the following properties.

We considered two possible arrangements for the cameras: a linear arrangement and a curved arrangement with piecewise linear properties over large scales. These camera topologies are shown in Figure 1. In both arrangements, the cameras are placed around the pitch at a certain height to allow an overview of the scene. Both the curved and linear arrangement use cameras with a fixed location and orientation. Some overlap between the camera images is required to allow feature matching. Overlap between every camera is, however, not required.

Our method requires that the cameras are synchronized at shutter level, i.e. all cameras take an image at the exact same time stamp. To provide this, we use a pulse generator that periodically transmits a triggering pulse to all cameras at the same time.

3 REPRESENTATION OF CAMERA PARAMETERS

In this section, we give an overview of projective cameras and their matrix representations, commonly used in computer vision applications.

A simple pinhole camera maps each 3D scene voxel to a corresponding 2D image pixel, through projection along the light rays traversing the pinhole. Any real camera with a lens and finite aperture follows this basic voxel-to-pixel mapping principle and can hence conveniently be modeled by an equivalent pinhole camera. We will assume that all cameras follow the pinhole projective camera model, as defined by Hartley and Zisserman (2003, page 6) and shown in Figure 2.

This projective process can be mathematically represented in matrix notation as follows. Consider

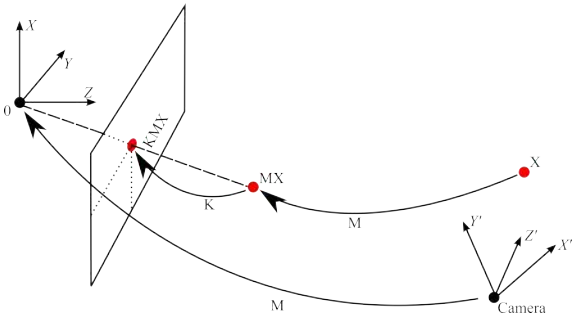

Figure 3: Intinsic and extrinsic camera matrices explained. The point χ and the camera center are defined in an arbitrary coordinate system. Multiplying by M will transfer the camera to the origin of the coordinate system, and χ will have the same relative position. Multiplying by K will project χ to the image plane.

a 3D point χ, represented in homogeneous coordinates. In essence, homogeneous coordinates represent a point $\chi = [X,Y,Z]^T$, using four coordinates $\chi = [WX,WY,WZ,W]^T$ with $W \neq 0$ or $\chi = [X,Y,Z,1]^T$. A projective camera now transforms this 3D point χ in a homogeneous 2D point $x = [x,y,1]^T$ using a projection matrix P:

$$x = P\chi \Leftrightarrow \begin{bmatrix} x \\ y \\ 1 \end{bmatrix} = P \begin{bmatrix} X \\ Y \\ Z \\ 1 \end{bmatrix}$$

Here, the projection matrix P can be split up in two sets of components: intrinsic and extrinsic parameters, represented by the intrinsic matrix K and the extrinsic matrix M, with $P = KM$.

The intrinsic camera parameters represent the relation between a 2D pixel location and its corresponding 3D ray, presuming the camera is placed at the origin, and the image plane is parallel to the XY plane at $Z = f$, where f is the focal distance. The line perpendicular to the image plane and passing through the center of projection is called the principal axis, while the point where the principal axis intersects the image plane is called the principal point. The principal point can be represented as a 2D point (p_x, p_y) on the image plane. The 3×3 matrix K is then given by:

$$K = \begin{bmatrix} f & 0 & p_x \\ 0 & f & p_y \\ 0 & 0 & 1 \end{bmatrix}$$

Using $x = K\chi$ for a camera placed at the origin with an image plane $Z = f$, x is the image coordinate on the image plane with principal point (p_x, p_y).

However, the camera is seldomly placed at the origin, especially if multiple cameras are involved. Therefore, the 3×4 extrinsic matrix M is used, which transforms 3D voxels to a new location and orientation, so that the intrinsic matrix K is applicable (Hartley and Zisserman, 2003, page 155). The matrix M consists of a rotation and a translation, as shown in Figure 3, and has the following form:

$$M = \begin{bmatrix} R & -R\tilde{C} \end{bmatrix}$$

where R is a 3×3 rotation matrix and $\tilde{C}$ is the camera location in non-homogeneous coordinates.

In essence, M will translate and rotate the world such that the camera is placed at the world origin, where K will then project the 3D voxels to the image plane, resulting in the final, projected image.

Using this camera model, the calibration process then consists of determining these projection matrices, when only the images of the cameras are given. To this end, we acquire image correspondences using feature matching, use them to generate the projection matrices, and then finally split these projection matrices into their intrinsic and extrinsic components using the QR decomposition (Hartley and Zisserman, 2003, page 579), which exploits the triangular shape of matrix K.

4 DETERMINATION OF 2D IMAGE CORRESPONDENCES

We determine image point correspondences by using a feature detector on all synchronously captured images individually, followed by all possible combinations of pairwaise matching. To increase robustness, feature matching between each pair of images is done in two directions, i.e. find the matches from image 1 to image 2, and cross-check with the matches from image 2 to image 1. A number of pairwise feature detectors were tested (Doshi et al., 2010), including the SIFT (Lowe, 2004) and SURF (Bay et al., 2006), where SIFT proved to provide the most reliable matches on our dataset.

The configuration of the cameras determine the exact approach for finding matches. If the cameras are far away from each other, only groups of three sequent cameras are considered to find matches. This avoids extreme outliers resulting from matches over images that contain a very different part of the scene. If the cameras are placed in an arc, one camera can have a view angle perpendicular to the view angle of another camera. This will make matching of features on players unreliable and is therefore avoided by using only three successive cameras.

If the cameras are close to one another and there is a large overlap between all cameras, matches between

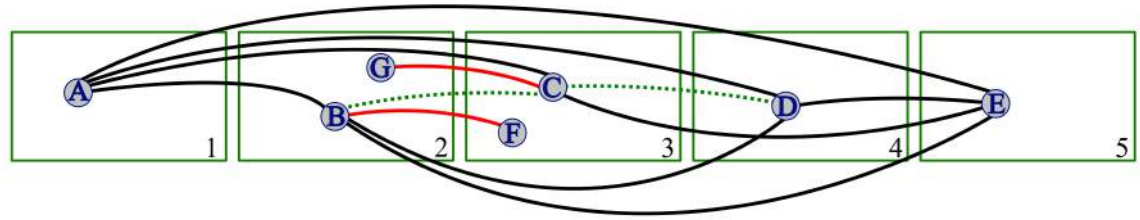

Figure 4: The graph used in our example. Nodes A - G are features detected in a set of images, each of which is taken by a different camera at the same moment. The red edges show mismatches between features, the black correct matches between features. The green, dashed lines show the feature matches that should have been found, but were not. After running our algorithm, A, B, D, E are considered as accepted in the multicamera feature match; C, F, G are rejected.

		From Camera				
		1	2	3	4	5
To camera	1	-	A	A	A	A
	2	B	-	G	B	B
	3	C	F	-	-	C
	4	D	D	-	-	D
	5	E	E	E	E	-

Figure 5: Resulting matrix of the example in Figure 4.

all pairs of images are searched for. We will select matches between all cameras using a consensus based searching approach.

For a multicamera match to qualify for use in calibration, it has to contain features of at least three cameras and the matching in each image pair has to be consistent, using the algorithm proposed in the next paragraphs. An overview of the algorithm is given in Algorithm 1.

The algorithm can better be explained using the example of Figure 4. Here, a graph is shown, where each node is a feature, belonging to a specific camera image, and each edge represents matching features in two directions. An edge between node A and B, corresponds to a match between feature A and feature B, and vice versa.

We consider every pair of images and decide which feature pair will be kept, and which will be discarded. We decide which other features in other images belong to this match, therefore creating a multicamera match. For example, we consider camera 1 and camera 2. One of the cameras is the primary camera C_p, the other is the subordinate camera C_s. We choose camera 1 as C_p. Next, we construct a feature cross check matrix for each feature F_p that is a part of a match between C_p and C_s. In our case, we consider feature A. The matrix consists of N rows and N columns (where N is the number of cameras) and each row and column corresponds to a camera image.

We now complete every element of the matrix. For each element there is a "from" camera C_f and a "to" camera C_t. First, we select the match from C_p to C_f, that is $C_p \leftrightarrow C_f$, and use this feature to find the match to C_t ($C_f \leftrightarrow C_t$). For $C_p = 1$ with feature A, $C_f = 4$ and $C_t = 5$, this would result in $A \leftrightarrow D$ and $D \leftrightarrow E$. The result is the final feature from the second match, and is placed in the matrix on row C_t and

Algorithm 1 Overview of the multicamera feature matching and selection algorithm.

```
Create empty list of multicamera matches L_m
for all Cameras C_p do
    for all Cameras C_s, C_p ≠ C_s do
        for all Feature F_p ↔ F_s of C_p ↔ C_s do
            Construct matrix M
            for all Cameras C_f do
                for all Cameras C_t do
                    if c_f = c_t then
                        M[C_f][C_t] = unset
                    else if c_f = c_p then
                        Match F_p ↔ F_2 in C_p ↔ C_t
                        M[C_f][C_t] = F_2
                    else
                        Match F_p ↔ F_2 in C_p ↔ C_f
                        Match F_2 ↔ F_3 in C_f ↔ C_t
                        M[C_f][C_t] = F_3
                    end if
                end for
            end for
            Create empty list of features L_l
            for all Rows in M do
                Select most occuring feature F_m
                if Occurrence of F_m ≥ N/3*2 then
                    Add F_m to L_l
                end if
            end for
            if L_l has at least 3 features then
                Add L_l to L_m
            end if
        end for
    end for
end for
```

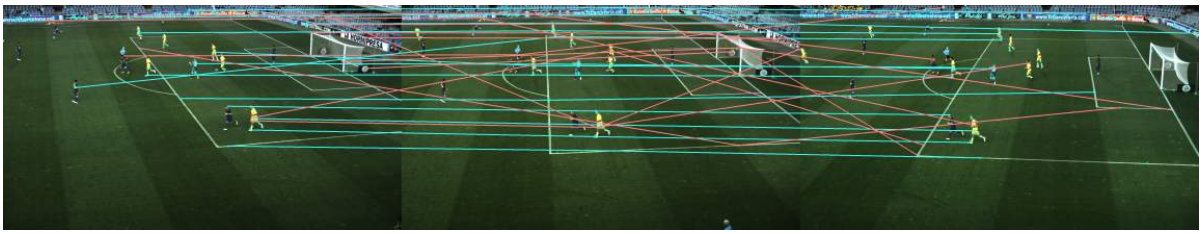

Figure 6: Example of multicamera feature matching using 3 cameras. All pairwise features are connected with each other using lines. Only a subset of the muticamera matches are shown, and the red mismatches will be removed later on in section 5.

column C_f. If there is no match, or if $C_f = C_t$, the position in the matrix is left empty. For our example in Figure 4, this results in the matrix shown in Figure 5.

There are several important elements worth noticing. First, as shown in Figure 4, there is no match between C and D, while there is a match $A \leftrightarrow C$ and $E \leftrightarrow C$, and a match $A \leftrightarrow D$, $B \leftrightarrow D$, and $E \leftrightarrow D$. Therefore, we can conclude that the match between C and D should exist (as indicated by the dashed green edge) and is just not found by the matching algorithm. Second, B matches to F, but both A and E match to both B and C. Furthermore, D matches to B. Therefore, we conclude that the match from B to F is a mismatch and should be eliminated. The same is true for $G \leftrightarrow C$. These two cases are handled by selecting the most occurring feature in each row.

To address the mismatches in Figure 4, we select the most occurring feature in each row and keep this feature only if it occurs more than two thirds of the time (including the empty places). For row 2, we see three times B and one time G. We can therefore consider B as part of the complete match, and ignore G. All rows in our example have a feature that is occurring two thirds of the time, except for the third row. Therefore, we will remove C (and F) from our multicamera feature set. Since C is only supported by two cameras, it is too weak to be considered as a reliable inlier, and is hence removed from the list.

By this method, we create a set of features for the feature from C_p, where we have calculated that they all presumably belong together. We will add this set of features to the global list of multicamera matches, after checking for duplicates. This process is repeated for every combination of C_p and C_s, and for every feature pair between these cameras.

An example for three cameras is shown in Figure 6. Here, 318 matches were found over 3 cameras. There were 2661, 3168, and 3011 matches in the three images resulting in 1171, 951, and 1088 matching features between pairs of images. By using the algorithm above, only 318 matches were retained, therefore yielding a higher robustness.

5 ANGLE-BASED 2D IMAGE CORRESPONDENCES SELECTION

Once the multicamera matches are determined, we perform an angle-based filtering which further enhances the correctness of the final result of the calibration by eliminating possible mismatches. The basis of this approach lies on the observation that correctly matched features in adjacent images have similar vertical displacement across images because our cameras are not rotated around the optical axis. More confidence is given to features that are more vertically "consistent" in adjacent images as large discrepancy in features' vertical position is a good indication of mismatch.

To perform a filtering based on this vertical displacement, we place a pair of images next to each other and connect all matches between these images. Next, we determine the angles between the horizontal and the lines connecting the features. Of these angles, we erase the top and bottom 5% and calculate the average of the remaining angle values. We will now discard any match of which the angle differs more than 3 degrees from the average. This parameter is determined empirically and can be adjusted if required. This is an effective outlier removal method, as demonstrated in Figure 7 and 8. Figure 7 shows the matches that passed the angle test. There are 288 matches, compared to the previous 318 matches. Most outliers are effectively removed, and no valid multicamera matches are erroneously removed. Figure 8 shows the matches where the angle test failed. All these matches are outliers, and are therefore removed from the succeeding calibration process.

This process is only applicable if the cameras are not too much rotated relative to each other, especially around the optical axis. If that were the case, the assumption that lines connecting matching features are more or less parallel would not be correct. For the linear camera arrangement, all cameras are set up such that they are upright relative to each other. For the

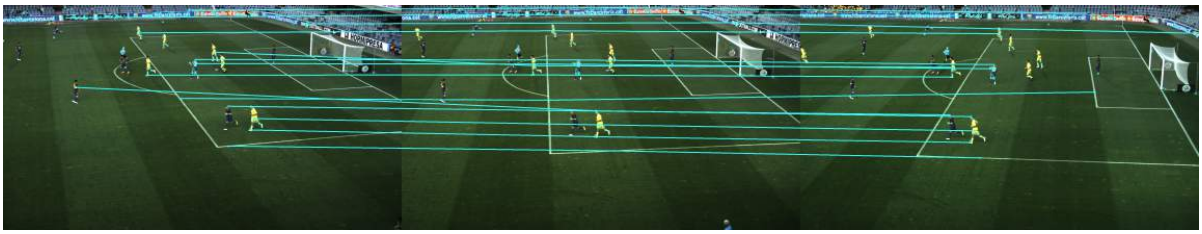

Figure 7: Multicamera feature matches, considered as inliers. Most outliers are removed using the angle-based filtering. Only a subset of the muticamera matches are shown.

Figure 8: Multicamera feature matches, considered as outliers. These matches were rejected using the angle-based filtering method. There are no false outliers in this example. Only a subset of the muticamera matches are shown.

curved camera arrangement, only 3 cameras are considered at a time, so that this angle-based selection remains effective.

6 CORRESPONDENCES TO PROJECTION MATRICES

Once the 2D correspondences are extracted and filtered, they are sent to the calibration toolbox of Svoboda et al. (2005). RANSAC (Hartley and Zisserman, 2003, page 117) is then used to further remove remaining outliers, and the projection matrices P are determined based on the correspondences using a bundle adjustment approach (Triggs et al., 2000)(Hartley and Zisserman, 2003, page 434).

Furthermore, radial distortion is determined (Hartley and Zisserman, 2003, page 189) and removed before the extraction of intrinsic and extrinsic matrices.

7 RESULTS

We verified the correctness of the calibration method by applying it to a real dataset of soccer games. We recorded three different soccer games using a multicamera setup, as shown in Figure 9. Some recorded images are shown in Figures 10 and 11. All cameras recorded the soccer game as described in section 2, and all cameras were synchronized. We extracted 10 images from the video stream at a rate of 1 image per minute. Using these sets of images, we apply the calibration method described earlier and verify the results, by simulating a plane sweep approach (Yang et al., 2003) and validating the relation between the depth hypothesis and the projection matrices P, defined in section 3.

In essence, an object in 3D space at a given depth plane in the scene will be projected to all camera views with their respective projection matrices P. Conversely, all the object's projected 2D images in the different camera views will coincide with one location in space, when performing the inverse projection P^{-1} towards the 3D object's depth plane. For instance, in Figure 12(a) the inverse projection of the yellow foreground player from the camera views towards his depth plane will bring all his projections in perfect overlap into a focused image, while all surrounding players at a different depth plane will present ghosting duplicates. A similar observation can be made for the focused blue background player of Figure 12(b) if the depth plane under test is put exactly at his 3D position.

It's worth noticing that the plane sweeping algorithm (Yang et al., 2003) exactly relies on testing different depth planes and detecting the focused image for estimating the object's depth. Given this depth information, we can now validate the camera calibration by estimating all the projection matrices P, and evaluate whether the inverse projections over all cameras provide an object in focus at the given depth plane. If not, at least one of the projection matrices would have been incorrectly evaluated.

The results for our datasets are shown in Figure 12. We have chosen a few depth planes that coincide

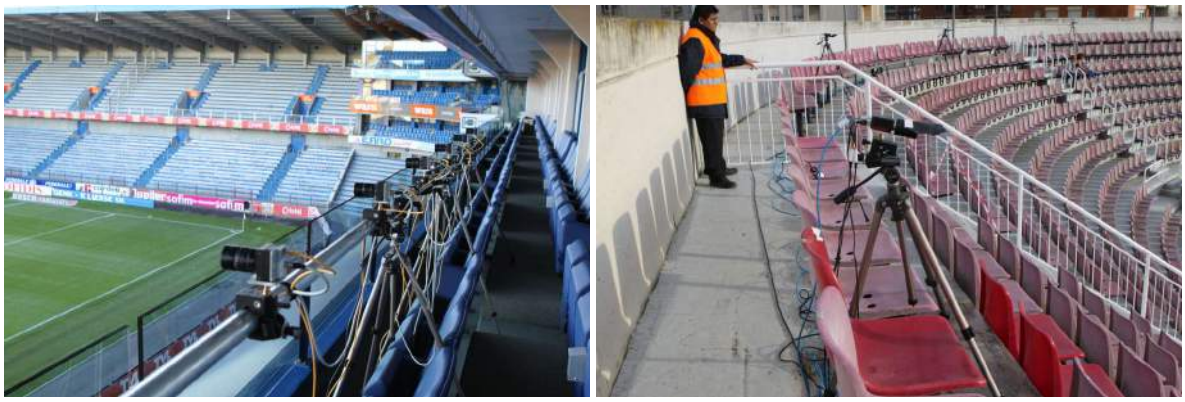

(a) (b)

Figure 9: The camera setup used to generate our datasets. (a) The linear setup. All cameras are placed on a line. (b) The curved setup. The cameras cover a quarter circle.

with players in the scene. The above described procedure brings the players at their corresponding depth plane always in focus. This demonstrates the correctness of our method and the applicability in reconstruction algorithms for soccer scenes (Goorts et al., 2013, 2014).

When using the multicamera matches without the angle-based selection, no valid calibration is returned by the calibration toolbox, clearly validating the usefulness of the approach.

8 CONCLUSION

We presented a method to generate multicamera feature correspondences for self-calibration in large scale camera networks, using existing calibration toolboxes. Pairwise feature matches are propagated over all camera views using a confident-based voting method. Features following a connecting line corresponding to the apparent movement across adjacent images are kept; all other features are considered as outliers and discarded. The remaining multicamera features can then reliably be used by existing calibration toolboxes, yielding correct camera calibration parameters. We demonstrated the quality of our method using a multicamera projection-based approach. Future effort will be directed to a more efficient approach and a more general filtering, i.e. allowing rotation of the cameras over the optical axes.

REFERENCES

Bay, H., Tuytelaars, T., and Van Gool, L. (2006). Surf: Speeded up robust features. In *Computer Vision–ECCV 2006*, pages 404–417. Springer.

Doshi, A., Starck, J., and Hilton, A. (2010). An empirical study of non-rigid surface feature matching of human from 3d video. *Journal of Virtual Reality and Broadcasting*, 7(10).

Farin, D., Han, J., and de With, P. H. (2005). Fast camera calibration for the analysis of sport sequences. In *Multimedia and Expo, 2005. ICME 2005. IEEE International Conference on*, pages 4–pp. IEEE.

Farin, D., Krabbe, S., Effelsberg, W., et al. (2003). Robust camera calibration for sport videos using court models. In *Electronic Imaging 2004*, pages 80–91. International Society for Optics and Photonics.

Goorts, P., Ancuti, C., Dumont, M., and Bekaert, P. (2013). Real-time video-based view interpolation of soccer events using depth-selective plane sweeping. In *Proceedings of the Eight International Conference on Computer Vision Theory and Applications (VISAPP 2013)*. INSTICC.

Goorts, P., Maesen, S., Dumont, M., Rogmans, S., and Bekaert, P. (2014). Free viewpoint video for soccer using histogram-based validity maps in plane sweeping. In *Proceedings of the Ninth International Conference on Computer Vision Theory and Applications (VISAPP 2014)*. INSTICC.

Grau, O., Prior-Jones, M., and Thomas, G. (2005). 3d modelling and rendering of studio and sport scenes for tv applications. In *Proceedings of WIAMIS*.

Hartley, R. and Zisserman, A. (2003). *Multiple view geometry in computer vision*, volume 2. Cambridge Univ Press.

Hayet, J.-B., Piater, J. H., and Verly, J. G. (2005). Fast 2d model-to-image registration using vanishing points for sports video analysis. In *ICIP (3)*, pages 417–420.

Li, Q. and Luo, Y. (2004). Automatic camera calibration for images of soccer match. In *International Conference on Computational Intelligence*, pages 482–485.

(a) (b) (c) (d) (e) (f)

Figure 10: Some frames from the input datasets. The cameras were placed in an arc setup at the top of the stadium. The cameras were aimed at the penalty area.

Lowe, D. (2004). Distinctive image features from scale-invariant keypoints. *International journal of computer vision*, 60(2):91–110.

Ohta, Y., Kitahara, I., Kameda, Y., Ishikawa, H., and Koyama, T. (2007). Live 3D Video in Soccer Stadium. *International Journal of Computer Vision*, 75(1):173–187.

Svoboda, T., Martinec, D., and Pajdla, T. (2005). A convenient multicamera self-calibration for virtual environments. *Presence: Teleoperators & Virtual Environments*, 14(4):407–422.

Thomas, G. (2007). Real-time camera tracking using sports pitch markings. *Journal of Real-Time Image Processing*, 2(2-3):117–132.

Triggs, B., McLauchlan, P. F., Hartley, R. I., and Fitzgibbon, A. W. (2000). Bundle adjustmenta modern synthesis. In *Vision algorithms: theory and practice*, pages 298–372. Springer.

Yang, R., Welch, G., and Bishop, G. (2003). Real-time consensus-based scene reconstruction using commodity graphics hardware. *Computer Graphics Forum*, 22(2):207–216.

Yu, X., Jiang, N., Cheong, L.-F., Leong, H. W., and Yan, X. (2009). Automatic camera calibration of broadcast tennis video with applications to 3d virtual content insertion and ball detection and tracking. *Computer Vision and Image Understanding*, 113(5):643–652.

Zhang, Z. (2000). A flexible new technique for camera calibration. *Pattern Analysis and Machine Intelligence, IEEE Transactions on*, 22(11):1330–1334.

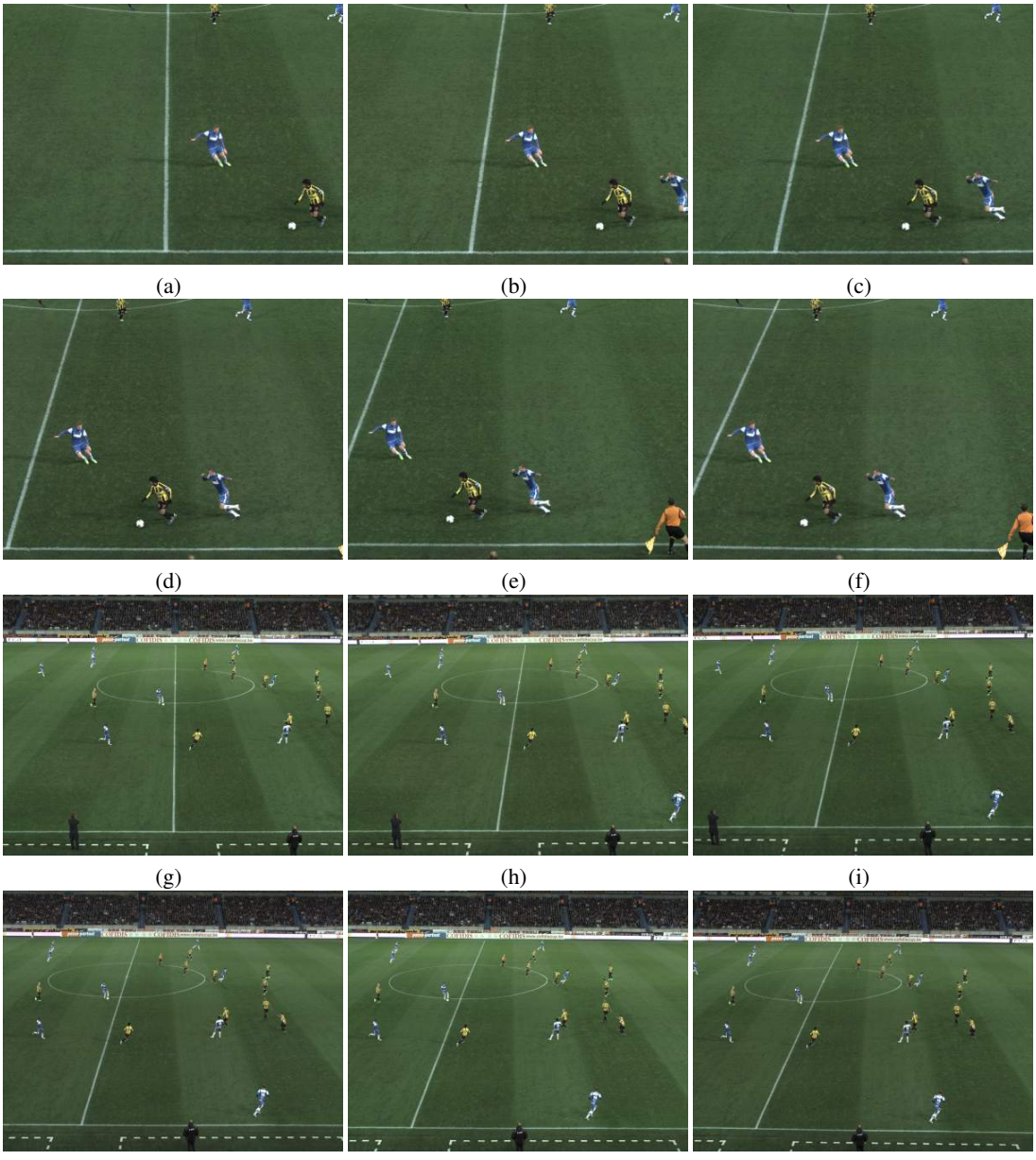

(a) (b) (c)

(d) (e) (f)

(g) (h) (i)

(j) (k) (l)

Figure 11: Some frames from the input datasets. The cameras were placed in a linear setup at the top of the stadium. Two focal lengths were used.

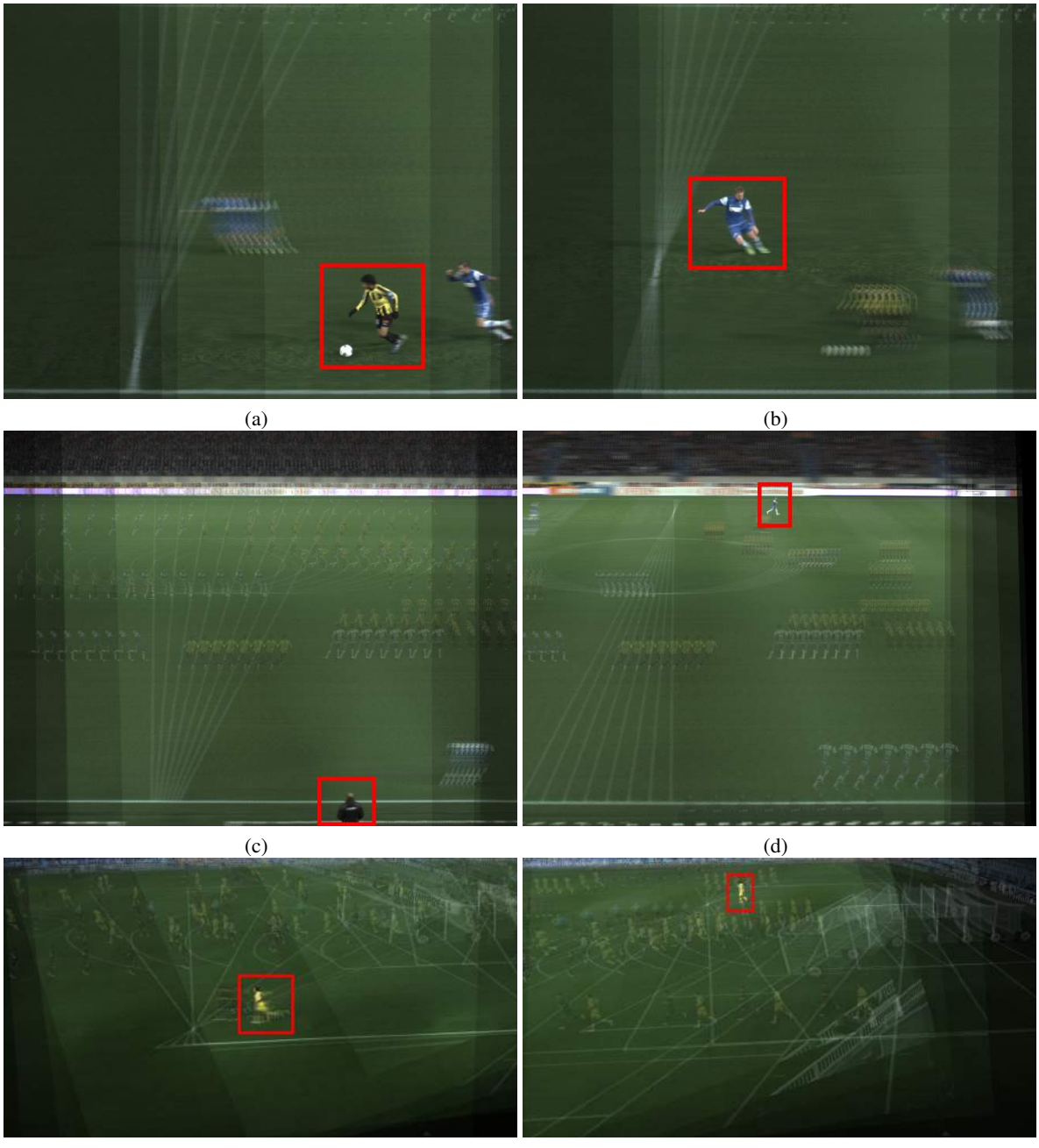

(a) (b) (c) (d) (e) (f)

Figure 12: Visual results of reprojecting the calibrated images to a plane in the scene. If the same object in every image projects to the same location on a single plane, then the camera calibration is correct. The images above show the projection for some planes on different depths. The objects in the red boxes all project to the same location, demonstrating the correctness of our method.